ENGINEERING SEMICONDUCTOR QUANTUM DOTS FOR QUANTITATIVE IMAGING OF CELL MOTILITY AND INVASION

BY

ANDREW XIN ZHAO

THESIS

Submitted in partial fulfillment of the requirements
for the degree of Master of Science in Materials Science and Engineering
in the Graduate College of the
University of Illinois at Urbana-Champaign, 2015

Urbana, Illinois

Adviser:

Assistant Professor Andrew Smith

ABSTRACT

Quantum dots (QDs) are photo-luminescent nanocrystals that possess unique optical properties such as a narrow emission range and high photo-stability, which makes them useful for a variety of biological imaging applications. In this study, QDs presenting different chemical moieties were used to quantify non-specific binding to different extracellular matrix (ECM) proteins. QDs coated with poly-maleic anhydride (PMA), which had been modified to present alkane, alkene, alkyne, PEG and carboxylic acid, carboxylic acid, and solely PEG, were incubated on poly-l-lysine, collagen, fibronectin, and gelatin coated glass coverslips. Based upon the emission intensity normalized by the quantum yield (QY), the binding of the QDs were directly compared. The QD coated substrates exhibited photoluminescent enhancement (PLE) resulting in an increased emission intensity when excited over time. Based upon this increase, a more accurate QY was calculated, allowing for proper comparison between the QDs. Different ECM proteins possessed different binding affinities to different chemical moieties. Poly-L-lysine was shown to bind well to PEG/carboxylic acid particles, but paradoxically, not as well to carboxylic acid. Collagen exhibited an affinity to the alkyne coated particles. Fibronectin showed high binding to PEG/carboxylic acid QDs, but also bound well to the alkane, alkene, and alkyne. Gelatin, like fibronectin, also showed affinity to most of the particles. Due to differences in the QY and PLE, the QDs that bound the most to each protein did not produce the most uniform and brightest substrates.

MDA-MB-231 human breast cancer cells were then seeded on gelatin substrates coated with the QDs for 24 hours. Evidence of uptake and degradation of the matrix was observed, but

could not be quantified using wide-field fluorescent microscopy. As a result, confocal images were required to properly characterize the degradation.

ACKNOWLEDGEMENTS

This project would not have been possible without support from members of Smith lab along with emotional support from friends and family. I would like to thank Professor Andrew Smith for providing guidance and ideas on the direction of the project. Liang Ma helped mentor and provided assistance on synthesizing the ligands, lyophilization, and NMR. Phuong Le provided vital assistance on coverslip coating and the degradation studies. Imaging on the TIRF system would not have been possible without Mohammad Zahid's assistance and support. I would also like to thank Sung Jun Lim for providing nanoparticles and suggestions, and Chunlai Tu for synthesizing the PEG ligand. I would also like to thank Kassidy Zhou for his assistance with some of the experiments.

I would like to also thank the Materials Science and Engineering Department at the University of Illinois at Urbana-Champaign for providing me with the opportunity to advance our scientific understanding and gain valuable training.

TABLE OF CONTENTS

ABBREVIATIONS ……vi

CHAPTER 1: INTRODUCTION ……1
1.1 Cell Motility and Metastasis ……2
1.2 Quantum Dots ……3

CHAPTER 2: LITERATURE REVIEW ……5

CHAPTER 3: METHODOLOGY ……7

CHAPTER 4: RESULTS AND DISCUSSION ……13

CHAPTER 5: CONCLUSIONS ……18

TABLES AND FIGURES ……20

REFERENCES ……32

ABREVIATIONS

DI water	De-Ionized water
DMAP	4-Dimethylaminopyridine
DMSO	Dimethyl Sulfoxide
ECM	Extracellular Matrix
FITC	Fluorescein Isothyiocyanate
FWHM	Full Width Half Max
I_C	X coordinate of the peak of a Gaussian Curve
NMF	N-Methylformamide
NMR	Nuclear Magnetic Resonance
PBS	Phosphate Buffered Saline
PEG	Polyethylene Glycol
PLL	Poly-L-Lysine
PMA	Polymaleic Anhydride
QD	Quantum Dot
QY	Quantum Yield
TIRF	Total Internal Reflectance Microscopy

TMAH	Tetramethylammonium Hydroxide
TRITC	Tetramethylrhodamine Isothiocyanate

CHAPTER 1: INTRODUCTION

In 2015, cancer is projected to have 1.6 million new cases and cause over 500,000 deaths in the United States alone.[1] Cancer originates from mutations within the cell's DNA that affect important pathways for homeostasis and cell proliferation.[2] Hanahan and Weinberg proposed that mutations leading to cancer could be classified under six traits, one of which is the development of an invasive phenotype for metastasis.[2]

Metastasis is the cause of over 90% of cancer deaths,[3] and it occurs when cancer cells leave the primary tumor and invade another organ. A prerequisite to this process involves the recruitment of blood vessels through angiogenesis, initially for growth factors and nutrients; eventually, the cancer cells are able to use the blood vessels as well as the lymphatic system as a highway to invade other areas in the body.[2] The metastasis process begins with cancer cells locally invading the surrounding area. Afterwards, through a process known as intravasation, cancer cells infiltrate into the blood stream or lymphatic system. The cancer cells then escape the vessel through extravasation, leading to growth and colonization of the organ.[4] By taking advantage of a process known as the EMT (epithelial-mesenchymal transition), cancer cells are believed to become migratory and degrade the epithelial basement membrane using invadopodia.[5] The EMT is a process by which epithelial cells develop a mesenchymal phenotype and is important for embryonic development and fibrosis in adults.[6] However, the process is believed to play an important role in metastasis as it imparts several traits such as increased invasiveness, resistance to apoptosis, and production of enzymes that mediate ECM degradation.[6] The complete degradation of the basement membrane signals the end of the

process, which is also observed in cancer cells during intravasation and metastasis.[7] The traits acquired through the EMT allow for cancer cells to remodel the surrounding ECM to enter the bloodstream and increase the chance of successful invasion and colonization of other organs.

Understanding the invasive nature of the cells and its relation to metastasis is important to identify potential targets to inhibit intravasation and the steps leading up to metastasis. This necessitates the need to study this initial process and the accompanying ECM degradation.

1.1 CELL MOTILITY AND METASTASIS

Cell motility and movement are dictated by the cell surface, shape, and position, such as membrane protrusions and retractions.[8] Changes in cell motility are intimately related to metastatic potential; the development of an invasive phenotype through the EMT is a result of changes in expression of adhesion proteins such as E-cadherin and N-cadherin and changes in the cytoskeleton.[9] In order for the cancer cells to invade the surrounding tissues, they must first degrade the ECM. The cancer cells use protrusions of the membrane called invadopodia, which are associated with proteins that allow for cellular motility, adhesion, and protease activity,[10] to degrade the ECM. Thus, targeting cell motility may be beneficial to limit local invasion, prevent further metastasis in patients with a metastatic cancer, and limit the development of a more metastatic phenotype.[11]

Various types of cell motility assays have been developed to track the cell membrane behavior such as cell attachment assays, rolling adhesion assays, chemotaxis chambers, and gel invasion.[12] Other methods for cell migration and invasion include the scratch assay, microfluidic devices, and cell exclusion zone assay.[13] The most relevant for studying cancer

migration are the chemotaxis chambers and the gel invasion. Chemotaxis chambers or transmembrane assays make use of a chemoattractant gradient and a membrane that only allows migrating cells to pass. However, this method is limited by the fact that the chemical gradient will equilibrate and the assay relies on counting of individual cells that cross an artificial membrane.[13]

Other methods include gel invasion assays are used to study migration and matrix degradation through the use of fluorophores conjugated to matrix proteins in either a hydrogel or deposited on a cover glass. As the cell spreads and migrates, it will degrade the surrounding matrix, releasing the fluorescent probe and leaving spots in the fluorescent substrate. This allows a quick comparison of migration among different cancer cell lines. However, this method cannot be used to image the cells in real-time as the dyes will photobleach.

1.2 QUANTUM DOTS

One exciting development in the field of imaging is the rise of quantum dots as a biological imaging tool. Quantum dots (QDs) are semiconducting nanocrystals typically made of Cd/Se/Zn/S that exhibit remarkable photostability, brightness, quantum yield, and narrow emission range.[14] These give QDs a significant advantage over traditional imaging probes such as dyes and fluorescent proteins, which lack the brightness; tend to photobleach, or decay upon prolonged exposure to light; and possess larger emission ranges.[15] These capabilities make QDs more suitable for long term imaging due to their photo stability, single molecule tracking due to their brightness, and multiplexed imaging due to their narrow emission ranges allowing for multiple QDs to be used simultaneously.

Cells have been observed to uptake QDs,[16] allowing for their use in cell motility assays. QDs allow for real time tracking of the cells, and additionally, if associated to the matrix, any matrix degradation will be typically followed by QD uptake. This can be used to compare the degree of degradation between cell lines based upon the amount of QDs that were uptaken.

For QDs to be relevant for biological studies, non-specific binding must be reduced or eliminated so that only the target molecule is bound by the QD. This makes it important to study the effects of different chemical moieties on non-specific binding to engineer a QD that will properly bind to the targeted ligand.

In this study, several QDs coated with poly-maelic anhydride derivative polymers are tested to determine the effect of different chemical moieties: alkane, alkene, alkyne, carboxylic acid, PEG and carboxylic acid, and PEG. Non-specific binding of the different QDs will be compared on the gelatin coverslips, and cells will be seeded on these substrates in hopes of observing the effect of these different moieties on cellular uptake.

CHAPTER 2: LITERATURE REVIEW

The earliest study of cell chemotaxis or invasion was performed by Professor Boyden who developed an assay to characterize leucocyte migration to a chemoattractant.[17] Termed the Boyden chamber, it consists of a chamber filled with chemoattratants and an insert with a membrane of a defined pore size that is placed above the chamber and filled with serum-free media. Cells are seeded in the top insert cannot pass through the membrane unless they are actively migrating towards the chemoattractant.

Though widely accepted, the Boyden chamber is time consuming, requires fixation, and does not allow for real time monitoring or condition variation.[16] Additionally, there are limitations to the invasive characterization of cancer cell using this assay. A study by de Both et al. showed that certain colon carcinoma lines (Caco-2, SW-480, SW-620, and HT029) did not migrate through the matrigel coated membranes in the Boyden chamber, while other carcinoma cell lines such as Colon-26 did.[18] This suggests that an alternative method is needed to test for invasiveness, such as a cell motility assay.

One example of a cell motility and degradation assay is the use of fluorescently labeled ECM proteins. The earliest example was performed by Mueller and Chen et al. where fluorescently labeled fibronectin coated gelatin beads were used to determine sites of invasion and uptake of the fluorescent protein were tracked.[19]

A different approach to the cell motility assay was described by Guenter Ablrecht-Buehler who used a glass substrate covered with gold particles to track the movement of NIH3T3 cells.[20] The cells were found to move upon the substrate and uptake the particles,

leaving a path behind them. The particles did not seem to change the normal morphology of the cells, and the uptaken particles appeared in the daughter cells, suggesting limited cytotoxicity. Abrecht-Buehler also showed that different cells had different migratory tracts. However due to the size of the gold particles (0.15 μm), the substrate coating was inhomogeneous, and the uptaken particles may perturb cell motility.[16]

Parak et al. showed that cancer cells uptake colloidal quantum dots that had been deposited on a collagen substrate.[16] The QDs were much smaller than the gold particles used by Albrecht-Buehler et al., possessing a diameter of 8 or 16 nm depending on the QD used. Unlike previously used fluorescent dyes, QDs do not photobleach as easily and can be imaged for longer periods of time. The cells uptook the QDs and, through confocal imaging, were found to clustered in the cytoplasm, likely in vesicles. MDA-MB-231 cells were noted to be extremely migratory, creating large non-fluorescent paths and uptaking large quantities of QDs.

Pellegrino et al. were the first to use QDs to characterize the invasive phenotype of different cancer lines. Glass was coated with collagen and silanized, water-soluble CDSe/ZnS QDs were deposited onto the surface. The glass was allowed to dry under UV light to create sterile the QD coated glass. Cell lines of normal breast epithelial cells (MCF 10A), breast tumor cells (MDA-MB-231, MDA-MB-435S, and MCF 7), colon tumor cells (SW 480), lung tumor cells (NCI H1299), and bone tumor cells (Saos-2) were compared based upon the non-fluorescent areas left on the QD layer, and the assay allowed the cancer cells to be classified as invasive and non-invasive. Invasive cells left a large trail of non-fluorescent areas, while non-invasive cells remained stationary and up-took QDs nearby the cell.[21]

CHAPTER 3: METHODOLOGY

All materials were purchased from Sigma Aldrich unless specified otherwise, and all cell culture materials were purchased from VWR unless stated otherwise. QD 600 with CdSe core with ZnS outer shell were synthesized in lab by Sung Jun Lim (see Figure 1 for absorbance and emission spectrum). Absorbance spectrum and quantum yield were measured using a Cary 5000 UV-Vis-NIR spectrophotometer and Horiba fluorometer. Images were taken on a Zeiss Laser TIRF 3 system. Gel doc XR system in the bio-nano lab in the Micro and Nanotechnology Lab was used to image the gels produced from gel electrophoresis.

Phase Transfer QDs to NMF: QD 600 stock solution (2 mL, QD 600 in 1-octadecene, oleylamine, and acetate) were diluted with chloroform (2 mL). Acetone (10 mL) was added drop-wise, resulting in flocculation, and the solution was centrifuged at 7000 g for 10 minutes. The supernatant was then discarded and the pellet was dissolved in hexane (5 mL). Methanol (2 mL) was added to extract out the excess polymers and removed via Pasteur pipette. More hexane was added until the volume returned to 5 mL. This was repeated a total of three times. The absorbance spectrum of the QDs was taken to calculate the concentration and number of moles of the QDs. The hexane solution was then placed in a vial with a stir bar and equal volume of NMF. TMAH (tetramethylammonium hydroxide, 26 µL per nano moles of QDs) was added, and the mixture was stirred at 400 rpm for an hour or until all the QDs transferred into the bottom NMF phase. The hexane was then removed and additional hexane was added; the solution was then stirred for five minutes. The hexane was removed, and the solution was

placed in a desiccation chamber to remove the remaining hexane by vacuum. Afterwards, the solution was centrifuged at 7000 g for 10 minutes to remove aggregates.

Ligand synthesis: Poly-maleic- anhydride (PMA, 100 mg) and DMAP (4-Dimethylaminopyridine, 2 mg) were dissolved in DMSO (0.5 mL) and purged with nitrogen three times. Histamine (66.65 mg or 0.7 mmoles) and 0.3 mmoles of the appropriate moiety containing an amine (alkane, propylamine; alkene, allylamine; alkyne, propargylamine; carboxylic acid, nothing; PEG and carboxylic acid, PEG-amine) were dissolved in 0.1 mL of DMSO and purged with nitrogen. The solution was then mixed with the PMA and DMAP solution and stirred overnight. The resulting solution was then dialyzed against 10 mM sodium hydroxide for 24 hours with 4-5 buffer changes and lyophilized. See Figure 2 for the chemical reaction.

The PEG ligand for the PEG particle was synthesized by Chun Lai Tu by polymerizing acrylic acid N-hydroxysuccinimide ester and mixing with TEG-NH_2 and histamine in DMF (see Figure 3 for the reaction schematic).

QD Coating: Coating was performed by dissolving the PMA derivative polymer (1.14 mg per nanomole of QD, 5 surface atom equivalents, 16 mg/mL) in NMF (n-methylformamide) and heating the polymer until it dissolved. The polymer solution was then added dropwise into QD 600 (conc. 1 µM, 2mL) in NMF while stirring. The solution was bubbled with nitrogen for five minutes, and heated at 110°C for 2 hours while stirring. After heating, the solution was allowed to cool to room temperature. 1 mM sodium hydroxide (1 mL) was added, and the solution was stirred for 10 minutes. The coated QD solution was concentrated using a 15 mL Amicon spin column (30 K) at 5000 g for 2 minutes and diluted in 50 mM sodium borate. The final solution

was then centrifuged at 7000 g for 10 minutes to remove any aggregates. The coating of the particle was confirmed using gel electrophoresis. The PEG polymer was coated in a similar manner except that the NMF QDs were diluted in five times their volume in DMSO and the polymer was dissolved in DMSO.

Gel electrophoresis: A 1% agarose gel was made by dissolving agarose (0.5 mg) in 50 mL of 50 mM sodium borate and microwaving for a minute, stopping to stir at after 15, 30, 40, and 50 seconds had elapsed. The solution was then left to cool for 5 minutes before pouring it into the mold and allowing the gel to solidify. The coated QD solution (10 µL, > 0.1 µM conc.) were then mixed with 2 µL of gel loading buffer (6 mL of glycerol, 12 mL DI water, and 2 mL of 500 mM sodium borate buffer) and loaded into each well in the agarose gel. The gel mold was then connected to a power supply and run at 110 V for 30 minutes.

Quantum Yield Measurement: The QD solutions were diluted to 0.15 µM and the absorbance spectrum was taken. Fluorescein was dissolved in 0.1 M sodium hydroxide and diluted such that the absorbance at 491 nm was similar to that of the QD solutions. The emission spectrum was obtained of both the QDs and the fluorescein solution by exciting at 491 nm. The quantum yield was then determined based upon the absorbance of the solutions at 491 nm and the emission spectrum.

FITC- Gelatin Conjugation: Gelatin was dissolved in pH 9.0 carbonate-bicarbonate buffer (10 mg/mL) and incubated at 37°C for 30 minutes. Afterwards, 10 µL of FITC dissolved in DMSO (10 mg/mL) was added to the gelatin and placed on a shaker table and allowed to react for an hour in the dark at room temperature. 2M glycine solution (100 µL) was added to quench

unreacted FITC for 10 minutes. The solution was then dialyzed against PBS in 1kDa MWCO tubing for two days with 4 buffer changes per day. The resulting gelatin mixture was then diluted to 0.2% and aliquoted into 0.7 mL microcentrifuge tubes and stored in the freezer.

ECM Protein Coverslip Coating: 18 mm glass coverslips (VWR) were placed in 20% nitric acid for 30 minutes. Afterwards, they were transferred into a 12 well plate and washed with DI water (1 mL) three times. The glass coverslips were then incubated with chilled poly-L-lysine (50 µg/ml in PBS, 1 mL) at room temperature for 20 minutes. The pol-L-lysine was then removed and the coverslips were washed three times with PBS. Chilled 0.5% glutaraldehyde (diluted from 70% stock solution) in PBS (1mL) was then incubated on the coverslips for 15 minutes at room temperature. The glutaraldehyde was removed and the coverslips were again washed three times with PBS. Gelatin solution (0.2% gelatin from porcine skin bloom 300 in PBS) was heated at 37°C for at least 30 minutes, and then the gelatin solution (0.5 mL) was incubated on the coverslips for 10 minutes. Fluorescent gelatin was conjugated in a similar fashion. FITC-gelatin was either used with or without dilution in 0.2% gelatin. The FITC-gelatin was used to confirm successful conjugation. Afterwards, the gelatin solution was then removed, and the coverslips was washed with PBS three times. The coverslips was then incubated with sodium borohydride (1 ml per well, 5 mg/mL) for 15 minutes on a shaker table to quench unreacted glutaraldehyde and decrease auto-fluorescence. The coverslips were again washed three times with PBS to remove any remaining sodium borohydride. Samples were then stored in PBS in the refrigerator at 4°C. Collagen I derived from rat tail and fibronectin derived from human plasma were coated in the same way but were not heated. For cell imaging purposes, an untreated four compartment, cell culture dish with glass bottom (VWR, 89125-444) was used and a

volume of 200 µL was used for incubation steps and 500 µL were used for wash steps. After coating, the cell culture dishes were placed in ethanol for at least 30 minutes to sterilize them.

QD association with ECM Protein: QDs were diluted with PBS to an appropriate concentration, either 100 nM, 50 nM, 25 nM, or 10 nM. The coverslips were incubated with 500 µL of the QD solution for 10 minutes or more depending on the experiment. The QDs were then removed and the coverslips were washed with PBS three times to remove unbound QDs. For the cell culture plates, the QD stock solutions were filtered with a 0.22 µm filter. The concentration of the QDs after filtration was determined and then the solution was diluted as appropriately. 200 µL of the resulting solution was then placed in each chamber and incubated for 10 minutes. The QD solution was then removed and the plates were washed with PBS (500 µL) three times.

Characterization of QD Bound ECM Protein Coated Coverslips: The coated coverslips were imaged by placing them onto coverglass instead of a glass slide and PBS (80 µL) was added onto the coverslips. The coverslips were exciting at 450-490 nm and using a 600 ± 15 nm filter to separate out the QD signal. Five images were taken at the center of the coverslip (see Figure 4). A histogram of the intensities was obtained from each image, which was fitted to a Gaussian curve. The peak intensity was divided by the quantum yield to create a direct comparison between different QDs.

Cell Culture and Staining: MDA-MB-231 cells were cultured in a T25 in DMEM supplemented with 10% FBS and 1% penicillin and streptomycin. Cells were passaged every three days using Trypsin-EDTA.

Cell Migration Assay: Cells were seeded on the QD and gelatin coated culture plates at 4000 cells/mL with 0.5 mL per chamber and incubated at 37°C for 24 hours. Afterwards the cells were fixed with 4% paraformaldehyde, and the nucleus of the cells were stained with Hoechst's stain. The culture plates were either imaged on the TIRF microscope or the LSM 700 Confocal at the Institute for Genomic Biology.

CHAPTER 4: RESULTS AND DISCUSSION

Quantum yield measurements of the particles, shown in Figure 5, show that the QDs using the PMA backbone possess similar QYs. Slight modifications in surface coatings result in modest changes of QY, with alkane QDs possessing the highest QY and PEG and carboxylic acid exhibiting the lowest QY. Likewise, the addition of PEG also seems to have decreased the QY when comparing the carboxylic acid QD to the PEG/carboxylic acid QD.

When characterizing the coverslips on the TIRF system, the QDs on the coverslips increased in brightness when excited overtime, increasing in intensity rapidly until reaching a peak. Afterwards, they slowly photo-decay or decrease in QY. This behavior agrees with the literature and is termed photoluminescent enhancement, typically occurring in thin films of QDs.[22] Though the exact mechanism of photoluminescent enhancement is not well understood, several possible explanations exist.

Photoannealing results in the brightening of QDs and is due to light transmitting heat, resulting in the annealing of bonds on the surface of the QD, however this can only occur in organic solvents.[23] PLE has been observed in CdSe QDs synthesized in water, which occurs in two stages. The first involves adsorption of water molecules during extended light exposure that increases in QY[24] due to the "passivat[ion of] surface charge-carrier traps, increasing the exciton emission."[23] The second stage involves the acceleration of the enhancement effect in the presence of oxygen, resulting in a blue-shift from the release of Cd^{2+} and the subsequent decrease in the QD diameter. Another possible mechanism is through photo-oxidation, which

involves electron transfer from the QDs to dissolved oxygen resulting in bluing and increase in QY.[23]

As the environment was not hypoxic and the QDs were in PBS, photo annealing is not possible. It may be possible that adsorption of water molecules resulted in the enhancement, however, no evidence of bluing of the QDs was observed.

In order to quantify changes in the QY, an image of the substrate was taken every 3.2 seconds from which a histogram of intensities would be obtained. Each histogram was fitted to a Gaussian curve, and the peak intensity of each curve were normalized by the peak intensity of the first image. The resulting change in intensities is shown in Figure 6. The changes in intensity correlate with the increase or decrease of the QY over time for each QD incubated at a concentration of 100 nM on PLL. Potential sources of errors would be due to variations in lamp intensity that may result in varying levels of excitement of the QDs. This is most prominently displayed in the 100 nM Alkane sample, where after 20 seconds, the intensities seem to vary significantly. However, the overall trend is still apparent. Most of the particles exhibit a logarithmic like growth and slow gradual decay.

The alkane QD exhibited the highest increase in signal (1.5x) compared to the other QDs, which plateaued between 1.1-1.25x of their original signal. The PEG/carboxylic acid QDs exhibited a slight increase in brightness followed by a gradual decrease to the initial intensity.

The excitation may be related to the surface ligands on the particle. The PEG particle, which features a different backbone polymer, shows a different trend when compared to the PMA based QDs. The PMA based QDs, excluding the PEG/carboxylic QDs, reach their max

intensity and begin to plateau between 20 to 40 seconds, while the PEG particle continues to increase past the measured time.

To obtain consistent results for accurate comparison among substrates, five images of the substrates were taken after the substrate seemed to reach the highest intensity or after 30 seconds of exposure. The peak intensities for each image would be determined and averaged. This value would be normalized to the peak intensity for the brightest QD for that substrate. The relative binding of the QDs on each matrix is shown in Figure 7. Surprisingly PEG/carboxylic acid QDs bound the most to PLL. This result is counterintuitive, as PLL is composed of many lysine amino acid residues that possess a positively charged amine. The carboxylic acid QDs, which possess a negative charge, were expected to bind the most to the positively charged substrate compared to the PEG/carboxylic acid particle, which theoretically possesses a lower negative charge and a large hydrophilic PEG chain. The charge effects may be reduced by the presence of sodium and calcium ions found in PBS, however, the ions only account for the charge and not the non-fouling properties of the PEG chains. As expected, the PEG QD shows little binding to the substrates, except for poly-l-lysine and collagen.

All the QDs tested exhibit some degree of binding to gelatin, with PEG exhibiting the least. Collagen on the other hand has a high binding affinity for alkyne QDs. Since gelatin is obtained through digestion of collagen, this result may suggests that the digestion disrupts the three dimensional structure of the protein that favors interactions with the alkyne moiety.

The uniformity of QD binding was determined using the FWHM from the Gaussian fit of the histograms used to determine QD binding. Similar to the binding calculation, the FWHM of

each substrate at a specific QD incubation concentration was determined by averaging the FWHM of five images of the sample. Figure 8 shows the results. The brightest samples exhibited the largest FWHM. This is likely due to the non-uniform illumination which is further exaggerated by the brighter QDs. Figure 9 demonstrates the correlation between brightness and uniform samples. Figure 9 A) shows an example of a moderately bright and uniform sample with the histogram of intensities. B) presents a highly uniform and dim sample, while C) is an extremely bright and un-uniform sample. QDs with high QYs that exhibit large degrees of photoluminescence enhancement further exaggerate the un-uniform excitation. Due to different QYs and degrees of photoluminescent enhancement, QDs that bind the most to each substrate are not necessarily the brightest and subsequently do not exhibit the highest FWHMs.

Based upon Figure 7, gelatin was selected for cell motility assays, due to the low cost and high binding affinity to most QDs. MDA-MB-231 were selected for their highly invasive phenotype. The cells were incubated for 24 hours on four-chamber, glass bottom, petri dishes that were coated in gelatin and incubated with different concentrations of each type of QD. The cells were then fixed. Initially, the TIRF system was used to image the fixed cells on the cell culture chambers. The acquired images are shown in Figure 10. These images corroborate the findings in Figure 7, in which the PEG particles exhibited the lowest levels of binding to gelatin. In Figure 10, the PEG/gelatin substrates exhibited little QD signal and appear similar to the control sample without QDs.

From these images, evidence of degradation is visible and are indicated by the arrows. However, the images do not possess the proper resolution to resolve exact tracks, necessitating the need to use confocal microscopy to properly observe the samples. Additionally, the

substrate associated with the cell appears brighter and seem to delineate the cell membrane. It is possible that increase in signal is due to uptaken QDs, but without confocal microscopy, it is not possible to definitively determine whether the signal originates from within the or underneath the cell.

Confocal images of cells incubated for 24 hours on the QD/gelatin coated cell culture chambers are shown in Figure 11. From the 3-D reconstructions, the QD signal is seen higher up in the cell and associate around the nucleus, stained by Hoechst, suggesting that the QDs uptaken into the lysosomes of the cell. This observation and conclusion is consistent the literature.[16] However, there is no clear evidence such as large non-fluorescent trails to show migration of the cells shown in other literature.[21] The visible degradation pattern resembles the small, punctate, non-fluorescent areas obtained through TRITC-gelatin degradation shown in Figure 12. The difference in the degradation may be due to different substrate and incubation conditions resulting in different phenotypic behaviors of the cells.

The confocal images also exhibit the same brightness patterns observed in the widefield images. The 3-d reconstructions and composite image suggest that the increased signal is not from within the cell as the uptaken QDs associate in clusters near the nucleus but from the substrate.

CHAPTER 5: CONCLUSIONS

In this study, QDs presenting different chemical moieties were used to test non-specific binding to different ECM proteins on a coverglass. It was found that different ECM substrates possess different degrees of non-specific binding depending on the presented chemical moieties. PEG and carboxylic acid QDs, paradoxically, bound the most to PLL. Alkyne coated QDs were found to bind the most to collagen, and all particles exhibited some degree of binding to gelatin, indicating that the digestion of collagen to form gelatin likely effected how the protein interacted with different chemical moieties. Fibronectin, like gelatin, did not seem to exhibit specific affinity towards any ligand. The highest binding affinity did not however, yield the brightest substrate. But due to non-uniform illumination, the brightest substrates exhibited the largest FWHM.

Evidence of degradation of the matrix was observed however, it could not be quantified using the wide-field imaging. But, signs similar to matrix degradation on hydrogels were observed. Images taken on the confocal microscope were not properly optimized, and as a result, the degradation could not be definitively determined. However, the cells did uptake the QDs, which associated near the nucleus, and the QDs seemed to associate with the cell membrane.

Follow up work should be done to optimize the proper conditions to observe migration of the 231 breast cancer cells. Another thing to investigate would be the apparent increased brightness of the QDs that is observed when the cells are sitting on them. Staining the cells with a membrane dye would help determine the location of the membrane in reference to the

brighter QD signal. Trypsinizing the cells after 24 hours and observing whether the bright patches are still visible can also be performed to determine whether the QDs associated with the membrane to produce the increased signal.

TABLES AND FIGURES

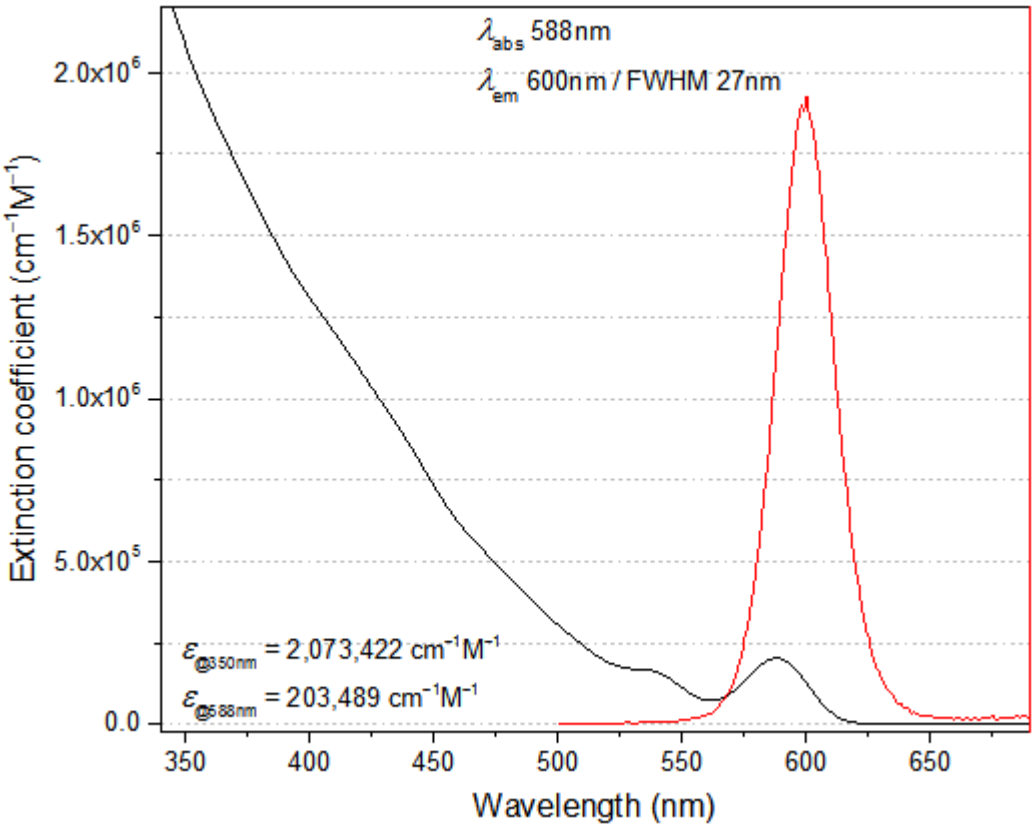


Figure 1. Absorbance and emission spectrum of QD 600 provided by Sun Jung Lim. The diameter of the QDs were 5.7 ± 0.5 nm.

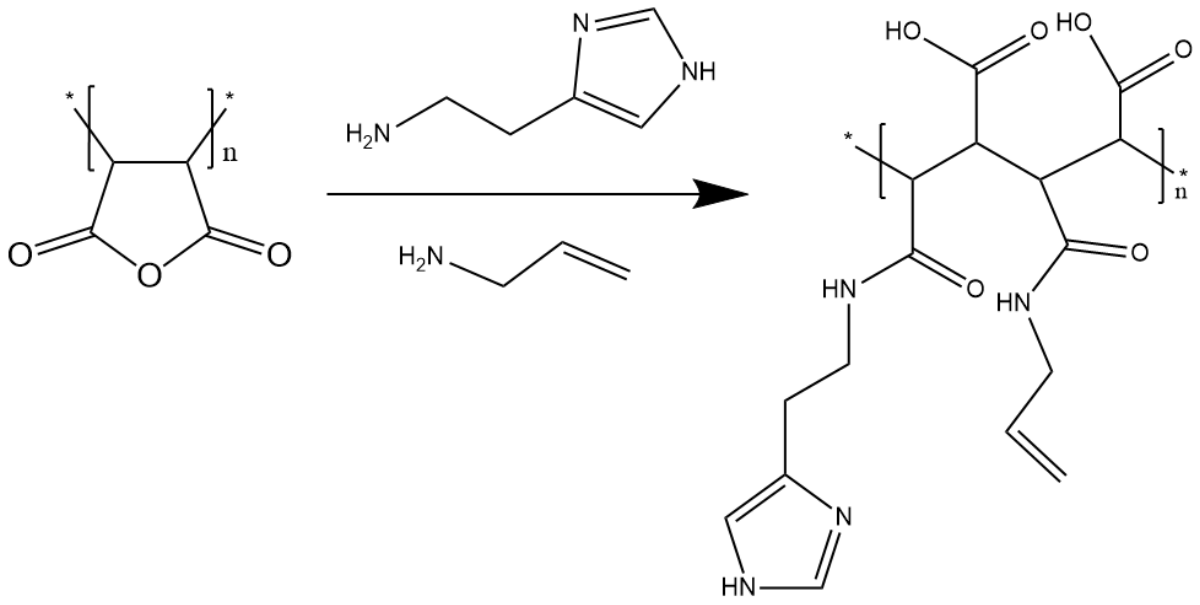


Figure 2. The schematic shows the reaction of poly-maleic anhydride with allylamine to form the alkene ligand. Replacing the allylamine with propylamine, propargylamine, or amine functionalized PEG will yield the alkane, alkyne, or PEG ligand respectively. Reacting the PMA backbone with 0.7 equivalent of histamine alone and neutralizing it in a basic solution of NaOH yields the carboxylic acid ligand.

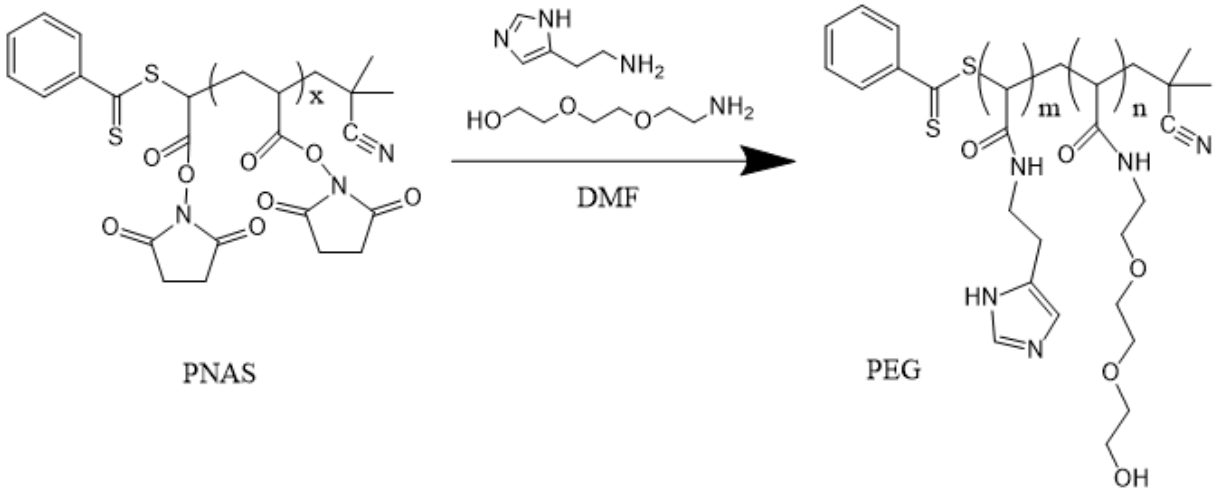


Figure 3. This schematic shows the reaction used by Chunlai Tu to synthesize the PEG particle. It varies from the other particles as it uses a different backbone, but as a result, contains no carboxylic acid groups.

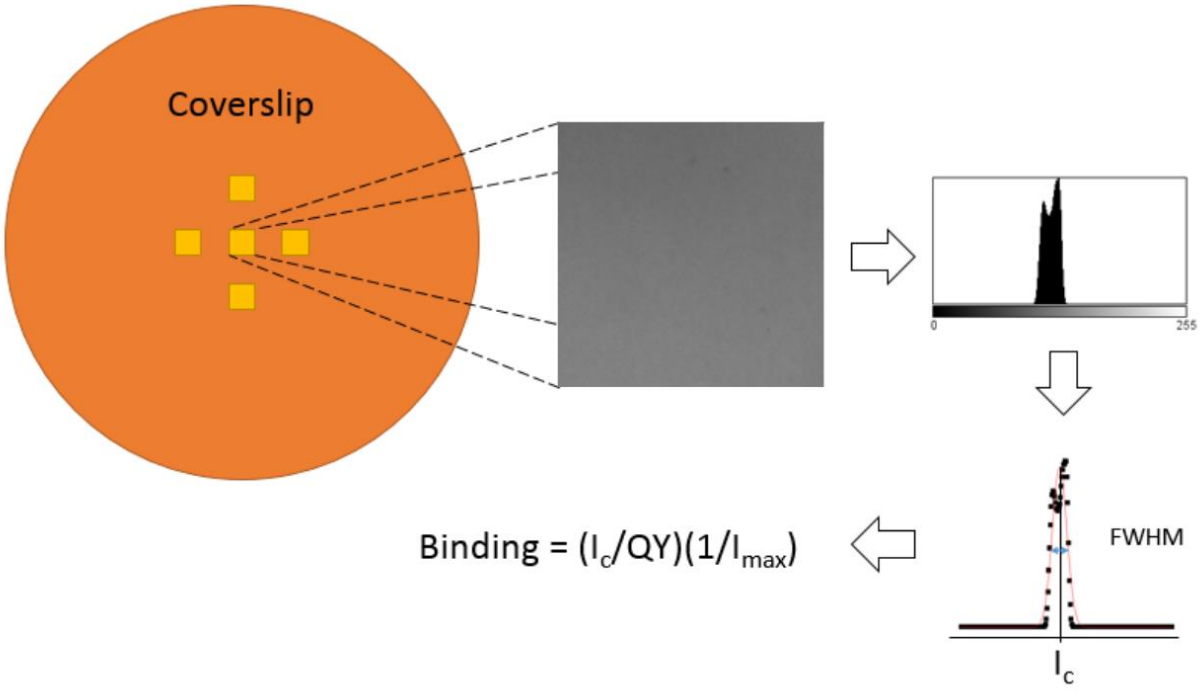


Figure 4. The schematic shows the locations on which the coverslip was imaged. A histogram of intensities was obtained and then fitted to a Gaussian curve. The two peaks are due to non-uniform illumination that results in the top part of the image to be dimmer than the bottom. The peak intensity of the fitted Gaussian was used to determine binding of the QD by normalizing by the quantum yield.

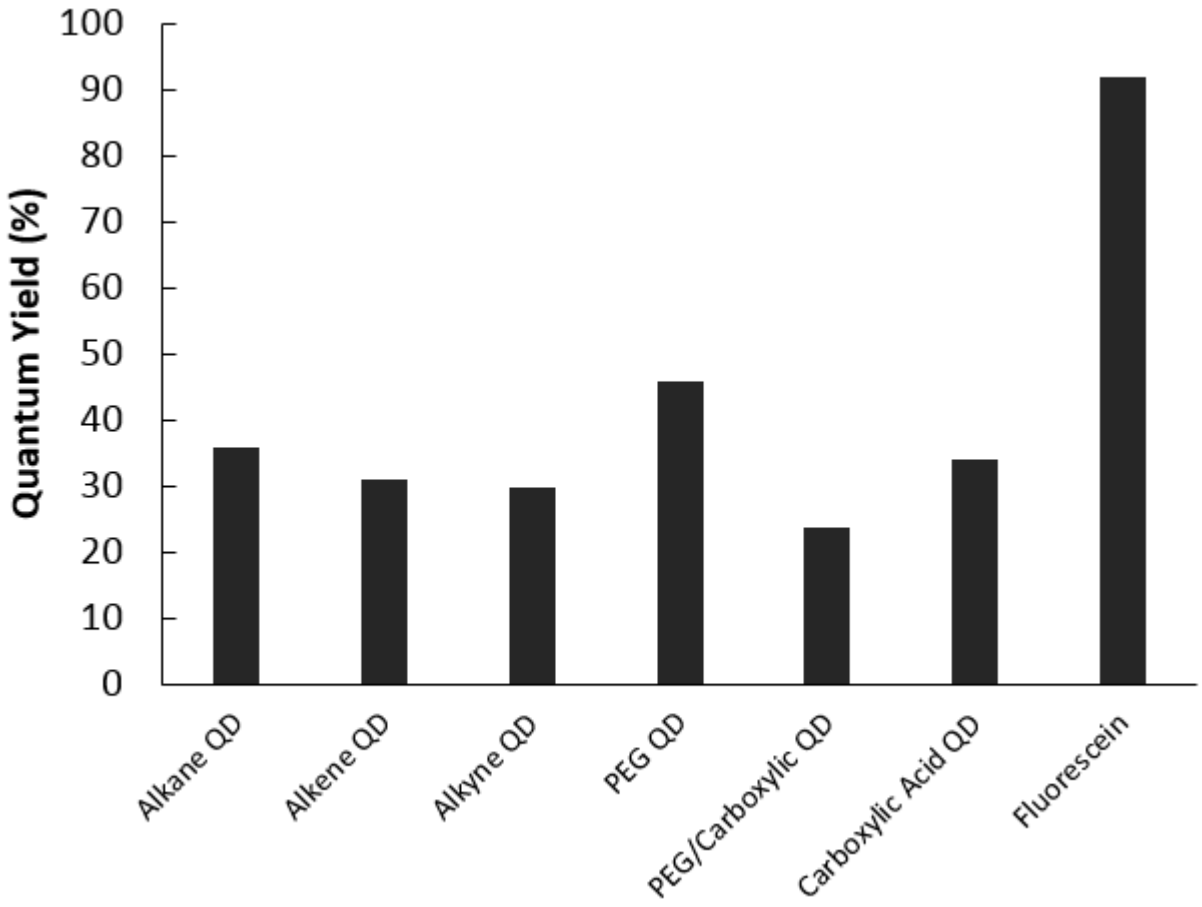


Figure 5. The quantum yield of each QD was determined using fluorescein as a reference dye. The QY values were used as a normalization factor to determine relative amounts of binding.

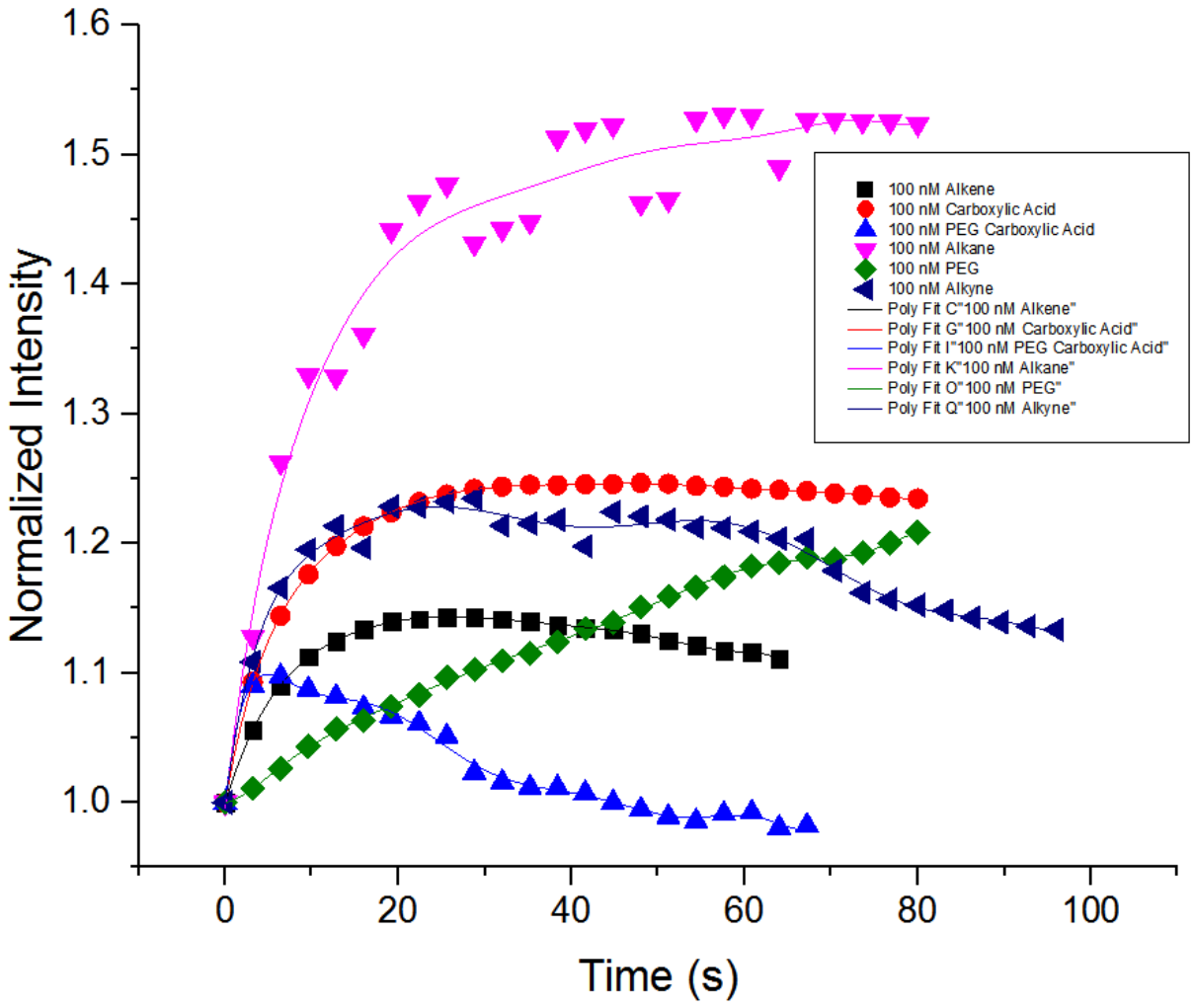


Figure 6. Images were taken every 3.2 seconds of each QD on a poly-l-lysine substrate that were incubated at a concentration of 100 nM. The peak intensity of each image is plotted against time. The increase in intensity reflects an increase in QY, which agrees with observations of photo luminescent enhancement. The QDs initially increase in brightness and plateau off before eventually photo-decaying.

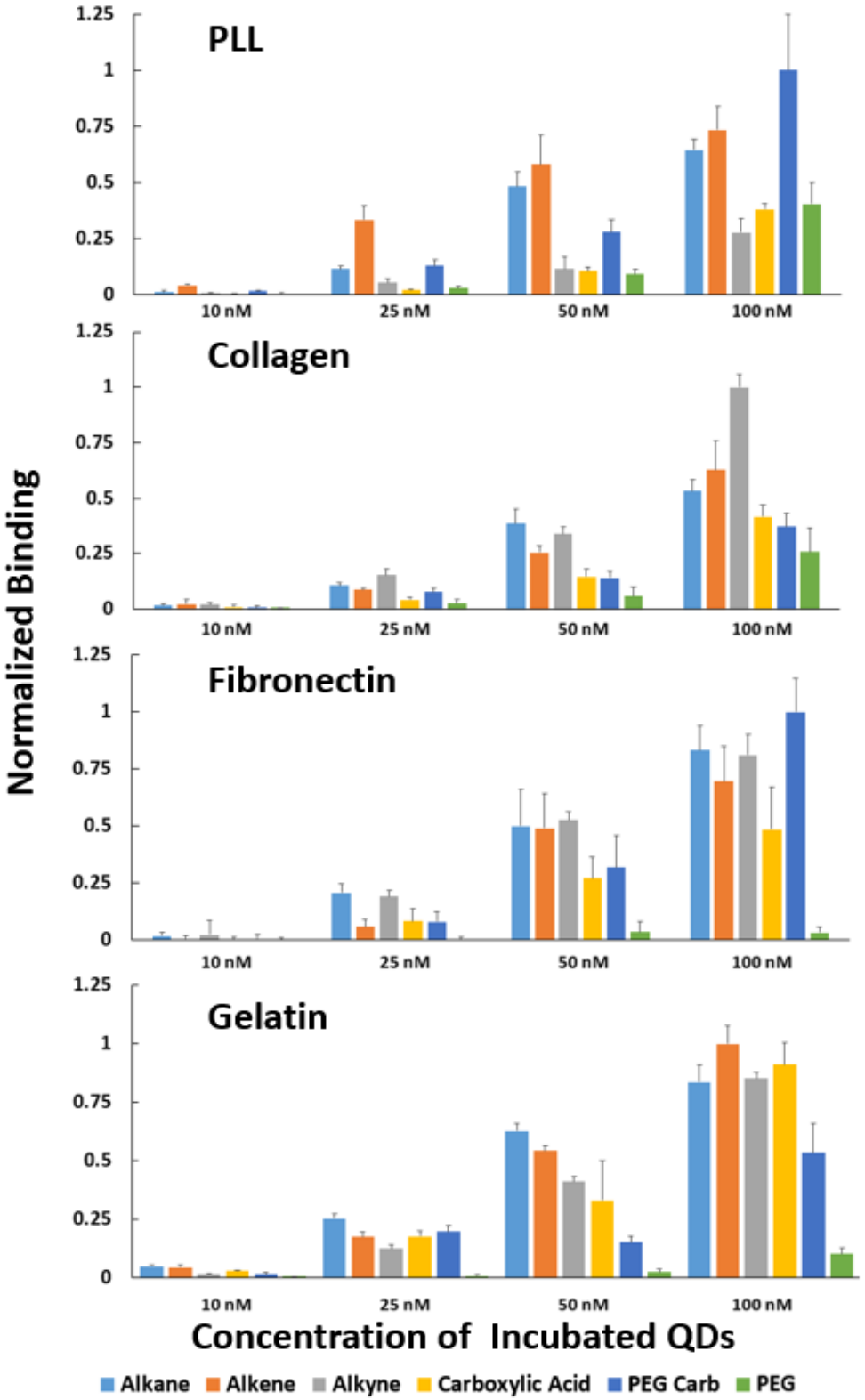


Figure 7. The bar graph shows the amount of binding of the QDs on to each ECM protein.

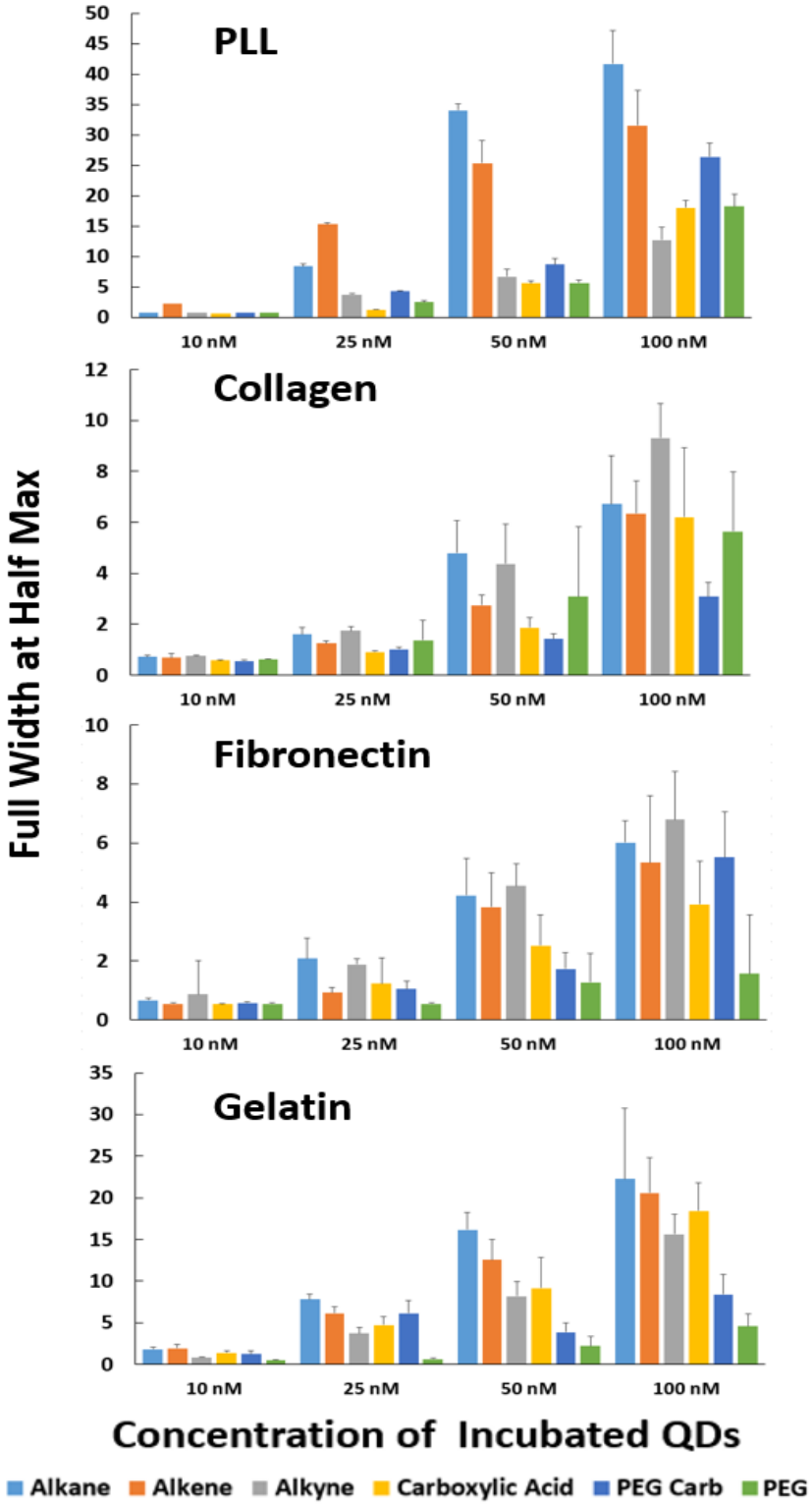


Figure 8. The bar graph shows the uniformity of binding onto each substrate. Lower FWHM values indicate more homogenous distributions.

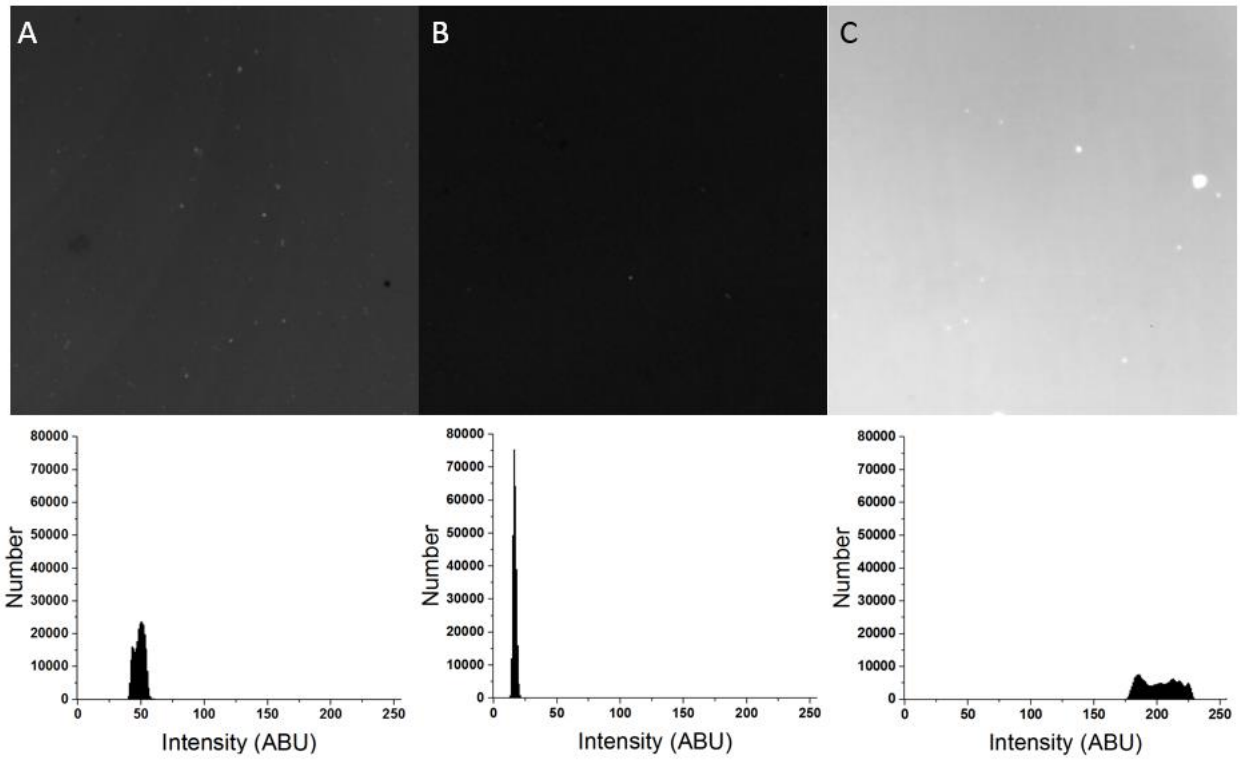


Figure 9. This figure shows the a correlation between in uniformity and brightness of the QD coated coverslips. A) is of 100 nM alkyne QDs on collagen, showing moderate brightness and uniformity. B) is of 100 nM PEG Carboxylic Acid QDs on collagen, which is considerably dimmer and more uniform. C) is of 100 nM alkane on PLL and is considerably brighter and less uniform. The non-uniform illumination is made apparent due to the high QY of the particle and high degree of PLE.

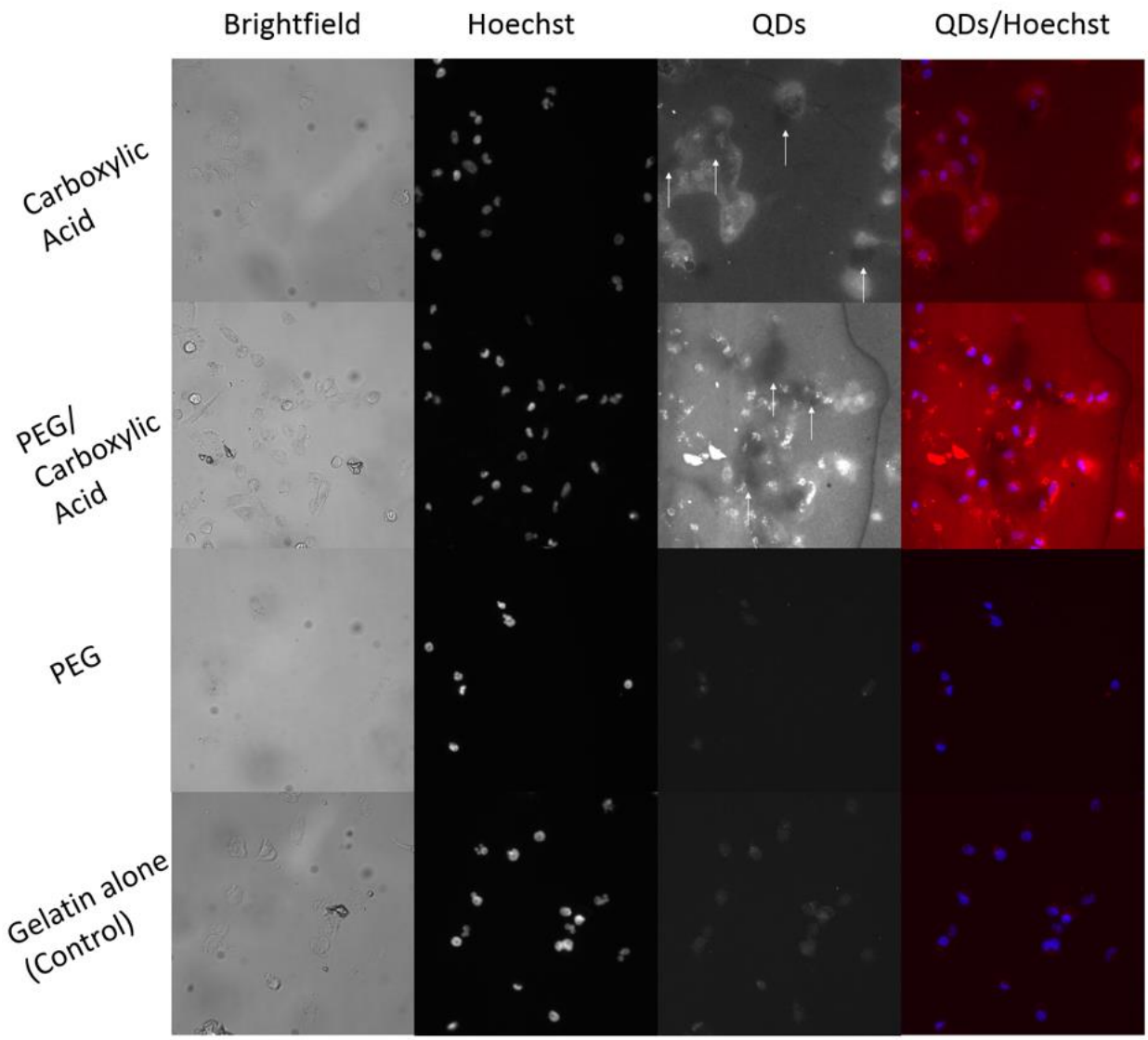


Figure 10. Wide-field images of the MDA-MB-231 cells on the QD coated gelatin substrates, with brightfield, Hoechst stain, red QD channel, and a composite of the QDs and the Hoechst channels. Evidence of trails, indicated by the white arrows, were observed but could not be quantified due to the large amount of cells and lack of clarity.

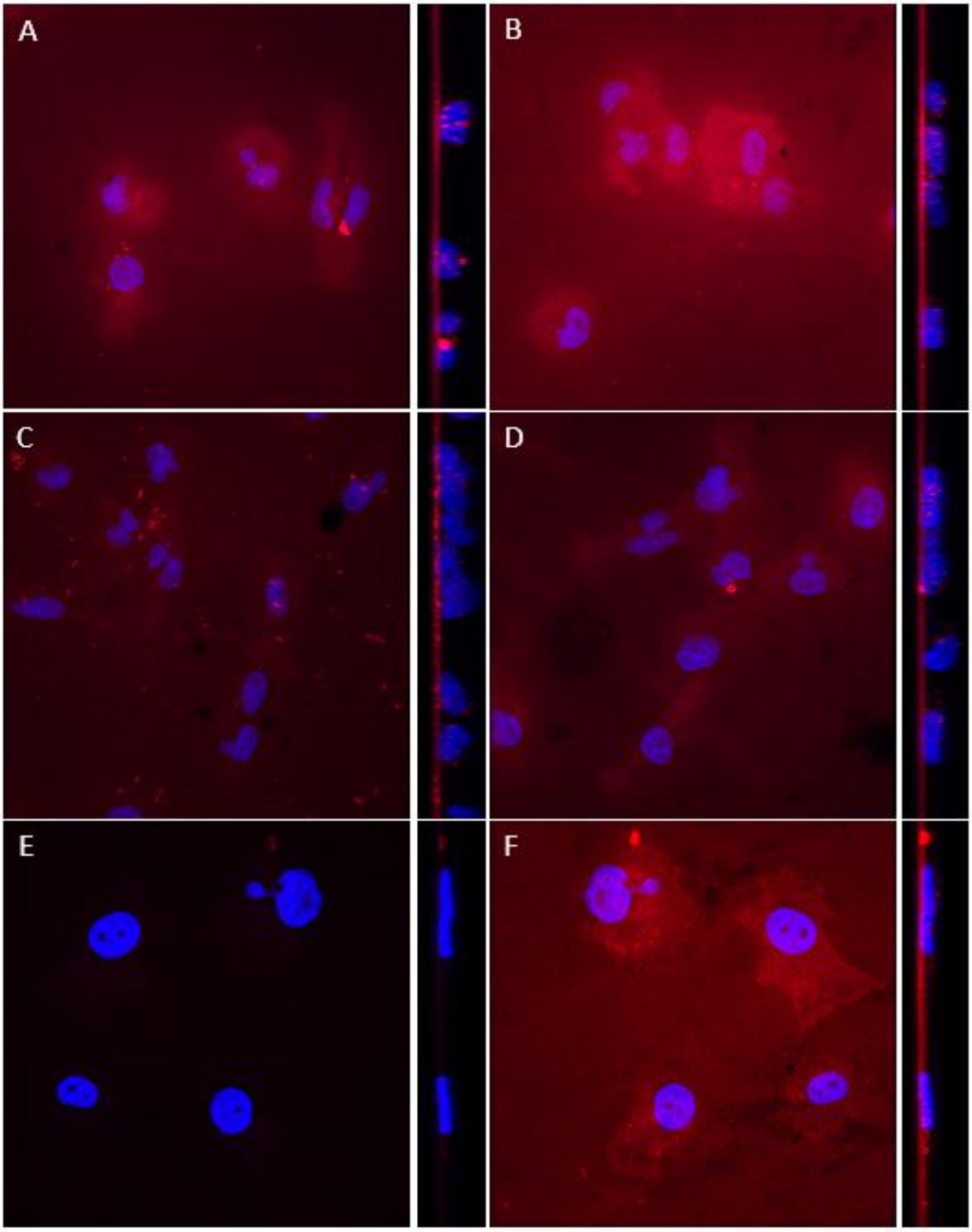


Figure 11. A) Alkane (B) Alkene (C) Alkyne (D) PEG Carboxylic Acid (E) Carboxylic (F) Carboxylic higher gain with a 3-d reconstruction on the right.

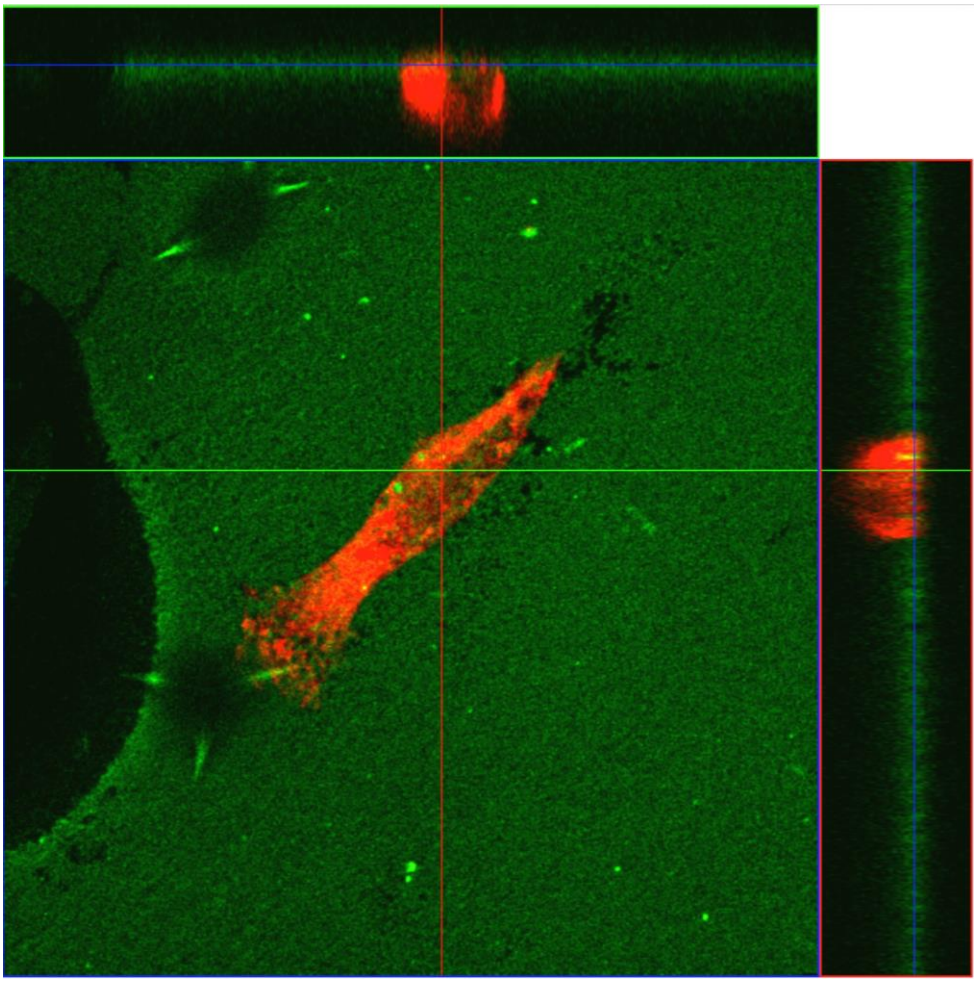


Figure 12. TRITC-gelatin degradation on a 10 kPa hydrogel provided by Phuong Le shows the expected degradation patterns.

References

1. Siegel, R. L., Miller, K. D. & Jemal, A. Cancer statistics, 2015. *CA. Cancer J. Clin.* **65,** 5–29 (2015).

2. Hanahan, D. & Weinberg, R. The hallmarks of cancer. *Cell* **100,** 57–70 (2000).

3. Mehlen, P. & Puisieux, A. Metastasis: a question of life or death. *Nat. Rev. Cancer* **6,** 449–58 (2006).

4. Hanahan, D. & Weinberg, R. a. Hallmarks of cancer: the next generation. *Cell* **144,** 646–74 (2011).

5. Bravo-Cordero, J., Hodgson, L. & Condeelis, J. Directed cell invasion and migration during metastasis. *Curr. Opin. Cell Biol.* **24,** 277–283 (2012).

6. Kalluri, R. & Neilson, E. G. Epithelial-mesenchymal transition and its implications for fibrosis. *J. Clin. Invest.* **112,** 1776–1784 (2003).

7. Gligorijevic, B. & Wyckoff, J. N-WASP-mediated invadopodium formation is involved in intravasation and lung metastasis of mammary tumors. *J. cell …* **125,** 724–34 (2012).

8. Sträuli, P. & Haemmerli, G. The role of cancer cell motility in invasion. *Cancer Metastasis Rev.* **141,** 127–141 (1984).

9. Kalluri, R. & Weinberg, R. The basics of epithelial-mesenchymal transition. *J. Clin. Invest.* **119,** (2009).

10. Buccione, R., Orth, J. D. & McNiven, M. a. Foot and mouth: podosomes, invadopodia and circular dorsal ruffles. *Nat. Rev. Mol. Cell Biol.* **5,** 647–57 (2004).

11. Palmer, T. D., Ashby, W. J., Lewis, J. D. & Zijlstra, A. Targeting tumor cell motility to prevent metastasis. *Adv. Drug Deliv. Rev.* **63,** 568–81 (2011).

12. Hague, A. & Jones, G. E. Cell motility assays. *Cell Biol. Toxicol.* **24,** 381–9 (2008).

13. Hulkower, K. I. & Herber, R. L. Cell migration and invasion assays as tools for drug discovery. *Pharmaceutics* **3,** 107–24 (2011).

14. Smith, A. & Nie, S. Chemical analysis and cellular imaging with quantum dots. *Analyst* 672–677 (2004).

15. Resch-genger, U., Grabolle, M., Cavaliere-jaricot, S., Nitschke, R. & Nann, T. Quantum dots versus organic dyes as fluorescent labels. **5,** 763–775 (2008).

16. Parak, W., Boudreau, R. & Gros, M. Le. Cell motility and metastatic potential studies based on quantum dot imaging of phagokinetic tracks. *Adv. Mater.* 2000–2003 (2002).

17. Boyden, S. The chemotactic effect of mixtures of antibody and antigen on polymorphonuclear leucocytes. *J. Exp. Med.* 453–466 (1962).

18. Both, N. De, Vermey, M., Dinjens, W. & Bosman, F. A comparative evaluation of various invasion assays testing colon carcinoma cell lines. *Br. J. Cancer* **81,** 934–941 (1999).

19. Mueller, S. & Chen, W. Cellular invasion into matrix beads: localization of beta 1 integrins and fibronectin to the invadopodia. *J. Cell Sci.* 213–225 (1991).

20. Albrecht-Buehler, G. The phagokinetic tracks of 3T3 cells. *Cell* **11,** 395–404 (1977).

21. Pellegrino, T. *et al.* Quantum dot-based cell motility assay. *Differentiation.* **71,** 542–8 (2003).

22. Lee, S. F. & Osborne, M. a. Brightening, blinking, bluing and bleaching in the life of a quantum dot: friend or foe? *Chemphyschem* **10,** 2174–91 (2009).

23. Carrillo-Carrión, C., Cárdenas, S., Simonet, B. M. & Valcárcel, M. Quantum dots luminescence enhancement due to illumination with UV/Vis light. *Chem. Commun. (Camb).* 5214–26 (2009). doi:10.1039/b904381k

24. Wang, Y. *et al.* Mechanism of Strong Luminescence Photoactivation of Citrate-Stabilized Water-Soluble Nanoparticles with CdSe Cores. *J. Phys. Chem. B* **108,** 15461–15469 (2004).